Robust voltage regulation for active distribution networks with imperfect observability

Edwin Mora & Florian Steinke
Energy Information Networks and Systems
Technical University of Darmstadt
Darmstadt, Germany
{edwin.mora, florian.steinke}@eins.tu-darmstadt.de

***Abstract*—This work targets voltage regulation in active distribution grids with imperfect observability due to limited communication and sensor equipment. Specifically, the on-load tap changer (OLTC) of distribution transformers, available voltage regulators, and few nodal reactive power injections are to be controlled in the presence of uncertainty about other nodal injections or voltage levels. The problem is solved with a novel two-stage, robust control approach for static linear systems with measurement-dependent uncertainty sets. The proposed ideas are demonstrated on small test feeders where OLTC positions are controlled based on local power flow measurements. More complex settings with additional sensors and actuators as well as robustness against a small number of significantly disturbed measurement signals are also shown. Results for the IEEE 123 test feeder prove the applicability to larger systems.**

***Index Terms*—Active distribution networks, robust control, voltage regulation.**

I. Introduction

The massive integration of decentralized energy resources into power distribution systems implies new challenges for the network operators in order to guarantee feasible system operation at all times [1]. In particular, the nodal voltage levels in the network are affected by decentralized generation and need to be actively regulated. The problem is known as the *voltage regulation* or the *Voltage VAr Control* (VVC) problem. It is challenging because the grid state is often highly uncertain due to a low number of sensors in the grid, which may or may not be connected to the control center.

VVC has been widely studied in recent years. With respect to the assumed degree of observability of the distribution grid, these works can be structured as follows. Many different actuators such as the OLTC of the main transformer, reactive power contributions of decentralized generators and capacitor banks, or voltage regulators can be controlled by solving central optimization problems targeting voltage feasibility at minimal losses and minimal switching frequency of the OLTC [2], [3]. The grid state is assumed to be fully known in these works. [4] estimates the grid state and accommodates for prediction errors by employing additional security margins for the controlled voltage levels. A stochastic optimization approach is followed in [5]. Robust control is considered in [6]. The considered uncertainty sets, however, are fixed and not adaptive to available measurement values. This means that the uncertainty set has to be larger than necessary and the control action more conservative.

In this work, we design robust control policies for the VVC problem. We make use of measurement dependent uncertainty sets which allows us to balance robustness and performance. Not only incomplete observability and measurement errors can be considered as sources of uncertainty but also the large scale failure of a small number of sensors, e.g., due to outages or malicious distortions.

Like [7], we formulate the setup as an abstract static linear system. However, we do not restrict ourselves to affine-linear controller structures but propose to use an online two-stage optimization approach. Given current values for the controlled variables we can quickly check whether an adaption is necessary, and otherwise save multiple costly OLTC switching events. Our principled, automated design approach can quickly adapt to changing system environments, e.g., in case of crises, and thus increases the operational resilience of the system.

The paper is organized as follows. Section II presents the adopted linear power flow model. In section III, we formally define the conditions for an admissible VVC control policy. Based on these conditions, we propose the novel control design method in section IV. The resulting controller is then applied to three different distribution feeders in section V, before we conclude in section VI.

II. Power system modeling

We adopt the linearized version of the *DistFlow* model [8] for balanced radial distribution networks without losses. Consider a radial network with $N+1$ nodes connected by N edges and let node 0 be the transformer of the distribution grid. At node i, the active and reactive power injections, and the voltage magnitude are denoted by p_i, q_i, and v_i, respectively. Moreover, p_{ik} and q_{ik} represent the active and reactive power flowing from node i to node k. Then,

This work was sponsored by the German Federal Ministry of Education and Research in project AlgoRes (grant no. 01|S18066A). It has been performed in the context of the LOEWE center emergenCITY.

$$
\begin{aligned}
p_{ik} &= -p_k + \sum_{k \to l} p_{kl}, \\
q_{ik} &= -q_k + \sum_{k \to l} q_{kl}, \\
v_i &= v_k + 2(\mathrm{r}_{ik} p_{ik} + \mathrm{x}_{ik} q_{ik}) + s_i.
\end{aligned} \tag{1}
$$

The sums are taken over all existing links from node k to node l. It is assumed that the link $i \to k$ has a series impedance given by $\mathrm{r}_{ik} + \mathrm{j}\mathrm{x}_{ik}$. The term s_i represents the effect of a voltage regulator at node i. If there is no voltage regulator at node i, we set $s_i = 0$ throughout.

Equations (1) are linear and the power flows p_{ik}, q_{ik} and nodal voltages v_i are determined uniquely by the combination of the power injections p_k, q_k at the non-root nodes, the voltage v_0 at the root node, and the voltage impacts s_i of the installed voltage regulators. We can thus call this combination of variables the *state* of the system. All other quantities of interest can be derived from it via a linear transformation.

In power grids, nodal voltages v_i are typically required to be maintained within the range of $[0.9, 1.1]$ p.u.. In order to guarantee such a feasible system operation, the OLTC of the distribution transformer at the root node can be controlled to set a voltage value v_0. Moreover, the reactive power injections q_k of some of the decentralized generators may also be available for actuation. These control actions can be determined based on local measurements at the root node, i.e., the total power supplied p_0, q_0, as well as information from some points throughout the grid, e.g., nodal voltage measurements v_i at some of the nodes with decentral generators. All state variables have physical limitations in the form of interval constraints. Additional constraints may apply in certain situations as outlined in the experimental section.

III. Admissible control laws

In line with [7], the described active distribution network model can be expressed as a constrained static linear system

$$
\mathbf{A}\boldsymbol{x} \leq \boldsymbol{b},\ \boldsymbol{y} = \mathbf{M}\boldsymbol{x}, \tag{2}
$$

with *state* vector $\boldsymbol{x} \subset \mathbb{R}^N$, *observation* vector $\boldsymbol{y} \subset \mathbb{R}^L$ that is available to the controller, and system parameters $\mathbf{A} \in \mathbb{R}^{K \times N}$, $\boldsymbol{b} \in \mathbb{R}^K$, and $\mathbf{M} \in \mathbb{R}^{L \times N}$.

State vector $\boldsymbol{x}$ can be partitioned into the *controlled* variables $\boldsymbol{x}_\mathrm{c}$, for which a control law is designed in the sequel, and the *free* variables $\boldsymbol{x}_\mathrm{f}$, that are left free to be determined either by other users, cooperative or malicious, by fixed external conditions, or at random. The value of $\boldsymbol{x}_\mathrm{c}$ is limited by lower and upper bounds, i.e., $\boldsymbol{x}_\mathrm{c}$ is an element of $\boldsymbol{\mathcal{X}}_\mathrm{c} = \{\boldsymbol{x}_\mathrm{c} : \boldsymbol{x}_\mathrm{c} \in [\underline{\boldsymbol{x}}_\mathrm{c}, \overline{\boldsymbol{x}}_\mathrm{c}]\}$. The vector $\boldsymbol{x}_\mathrm{f}$ is an element of the uncertainty set $\boldsymbol{\mathcal{X}}_\mathrm{f}$, which is presupposed to be a convex polyhedron. The defined partition of $\boldsymbol{x}$ allows to partition the matrices $\mathbf{A}$ and $\mathbf{M}$ along their columns, which yields $\mathbf{A}_\mathrm{c}\boldsymbol{x}_\mathrm{c} + \mathbf{A}_\mathrm{f}\boldsymbol{x}_\mathrm{f} \leq \boldsymbol{b}$ and $\boldsymbol{y} = \mathbf{M}_\mathrm{c}\boldsymbol{x}_\mathrm{c} + \mathbf{M}_\mathrm{f}\boldsymbol{x}_\mathrm{f}$. We in addition define $\boldsymbol{y}_\mathrm{f} = \mathbf{M}_\mathrm{f}\boldsymbol{x}_\mathrm{f}$.

We are interested in finding a control law $\boldsymbol{x}_\mathrm{c}(\boldsymbol{y}_\mathrm{f})$ that can guarantee feasible system operation, independently of the state of the free variables $\boldsymbol{x}_\mathrm{f}$. A controller satisfying this condition is said to be *admissible* [7]. This is formalized as follows.

Definition 1 (Admissibility)**.** *The control law* $\boldsymbol{x}_\mathrm{c}(\boldsymbol{y}_\mathrm{f}) : \mathbf{M}_\mathrm{f}(\boldsymbol{\mathcal{X}}_\mathrm{f}) \to \boldsymbol{\mathcal{X}}_\mathrm{c}$ *is admissible if*

$$
\forall \boldsymbol{x}_\mathrm{f} \in \boldsymbol{\mathcal{X}}_\mathrm{f} :\ \mathbf{A}_\mathrm{c}\boldsymbol{x}_\mathrm{c}(\boldsymbol{y}_\mathrm{f}) + \mathbf{A}_\mathrm{f}\boldsymbol{x}_\mathrm{f} \leq \boldsymbol{b}. \tag{3}
$$

Note that, without loss of generality, we take $\boldsymbol{y}_\mathrm{f}$ as the argument for the control law. This allows us to simplify the design of the controller as shown in the following. However, one could easily rewrite the control law into the form $\boldsymbol{x}_\mathrm{c}(\boldsymbol{y})$ since $\boldsymbol{y}_\mathrm{f} = \boldsymbol{y} - \mathbf{M}_\mathrm{c}\boldsymbol{x}_\mathrm{c}$.

In this work, we aim at finding an admissible controller $\boldsymbol{x}_\mathrm{c}(\boldsymbol{y}_\mathrm{f})$. This is a challenging task due to the all-quantor operating on $\boldsymbol{x}_\mathrm{f} \in \boldsymbol{\mathcal{X}}_\mathrm{f}$. In [7], we restricted possible controllers to an affine-linear form which allows to develop such controllers efficiently with the help of a suitable bounding strategy. However, it can be shown by example that for some situations no admissible affine-linear controller exists, whereas non-linear controllers can fulfill all requirements. We thus develop a novel framework for developing such non-linear controllers based on measurement-dependent uncertainty sets in the following.

IV. Design of Robust Non-linear Controllers

In order to find the admissible controller, we propose the following two-stage approach:

A. Stage 1: Task-Specific Characterization of Uncertainty Set

For a given measurement $\boldsymbol{y}_\mathrm{f}$, we first determine the values $\boldsymbol{x}_\mathrm{f} \in \boldsymbol{\mathcal{X}}_\mathrm{f}$ that maximize the impact on each system constraint while also yielding a $\boldsymbol{y}_\mathrm{f}$ measurement. To this end, let $\mathbf{A}_\mathrm{f}^i$ denote the i-th row of $\mathbf{A}_\mathrm{f}$. Also let $\overline{\boldsymbol{z}}_\mathrm{f} \in \mathbb{R}^K$ be the vector whose i-th entry corresponds to the maximum possible value of $\mathbf{A}_\mathrm{f}^i\boldsymbol{x}_\mathrm{f}$ consistent with $\boldsymbol{y}_\mathrm{f}$. I.e., for $i \in \{1, ..., K\}$,

$$
\begin{aligned}
\overline{z}_{\mathrm{f},i} = \max_{\boldsymbol{x}_\mathrm{f} \in \boldsymbol{\mathcal{X}}_\mathrm{f}} & \mathbf{A}_\mathrm{f}^i \boldsymbol{x}_\mathrm{f} \\
\text{s.t. } & \boldsymbol{y}_\mathrm{f} = \mathbf{M}_\mathrm{f}\boldsymbol{x}_\mathrm{f}.
\end{aligned} \tag{4}
$$

Expression (4) is a linear optimization task that can be solved very efficiently. Note first that the considered uncertainty set is measurement-dependent. It is typically smaller than the full set without considering the available measurements. Thus we can obtain less conservative controls below. Moreover, we do not need to compute all extremal points of the uncertainty set but only those with maximal impact on the constraints. Since the number of all extremal points of the uncertainty set scales exponentially with the dimension of $\boldsymbol{\mathcal{X}}_\mathrm{f}$ but the number of constraints is fixed and finite, this is a key step to render the approach computationally feasible.

B. Stage 2: Robust Control Computation

Once the entries of $\overline{\boldsymbol{z}}_\mathrm{f}$ are determined, a value for $\boldsymbol{x}_\mathrm{c}$ has to be determined such that $\mathbf{A}_\mathrm{c}\boldsymbol{x}_\mathrm{c} + \overline{\boldsymbol{z}}_\mathrm{f} \leq \boldsymbol{b}$. Note that such a value for $\boldsymbol{x}_\mathrm{c}$ will guarantee the fulfilling of the operational constraints for all possible realizations of $\boldsymbol{x}_\mathrm{f}$ associated to the measurement $\boldsymbol{y}_\mathrm{f}$. Although there are often multiple feasible

choices for $\boldsymbol{x}_\mathrm{c}$, we propose to choose the value that maximizes the distance β to a constraint violation, for all constraints. I.e., we solve the linear program (LP)

$$\begin{aligned} &\min_{\boldsymbol{x}_\mathrm{c},\beta} \ \beta \\ &\text{s.t. } \mathbf{A}_\mathrm{c}\boldsymbol{x}_\mathrm{c} + \overline{\boldsymbol{z}}_\mathrm{f} \leq \boldsymbol{b} + \beta, \\ &\quad \underline{\boldsymbol{x}}_\mathrm{c} \leq \boldsymbol{x}_\mathrm{c} \leq \overline{\boldsymbol{x}}_\mathrm{c}. \end{aligned} \tag{5}$$

If $\beta < 0$, the computed control $\boldsymbol{x}_\mathrm{c}$ is admissible. The computed value of $\boldsymbol{x}_\mathrm{c}$ may still be valid for another measurement $\boldsymbol{y}'_\mathrm{f}$, yielding another $\overline{\boldsymbol{z}}'_\mathrm{f}$, as long as $\mathbf{A}_\mathrm{c}\boldsymbol{x}_\mathrm{c} + \overline{\boldsymbol{z}}'_\mathrm{f} \leq \boldsymbol{b}$ still holds. This property is exploited next to compute values for $\boldsymbol{x}_\mathrm{c}(\boldsymbol{y}_\mathrm{f})$ over time.

C. Minimal Action Sequential Control

In practice, the controlled variables $\boldsymbol{x}_\mathrm{c}$ are often computed periodically based on the current measurements $\boldsymbol{y}_\mathrm{f}$ in order to adjust the system to new situations. However, it is not desired to adapt the OLTC voltage at each iteration due to economic and technical reasons. We therefore propose to adapt an existing $\boldsymbol{x}_\mathrm{c}$ *only* if its current value leads to a constraint violation. In each iteration, the current measurement $\boldsymbol{y}$ is read, which allows to calculate $\boldsymbol{y}_\mathrm{f} = \boldsymbol{y} - \mathbf{M}_\mathrm{c}\boldsymbol{x}_\mathrm{c}$. After solving the LP (4), we can compute how far each constraint is from being violated,

$$\boldsymbol{\theta} = \mathbf{A}_\mathrm{c}\boldsymbol{x}_\mathrm{c} + \overline{\boldsymbol{z}}_\mathrm{f} - \boldsymbol{b}. \tag{6}$$

If $\max_i \theta_i \leq 0$, then $\boldsymbol{x}_\mathrm{c}$ still fulfills the constraints of the system and no adaptation step is required. Otherwise, $\boldsymbol{x}_\mathrm{c}$ is adapted by solving LP (5).

A further option to speed up the iterative control loop in cases where $\boldsymbol{y}_\mathrm{f}$ is low-dimensional is to precompute all possible values $\boldsymbol{x}_\mathrm{c}(\boldsymbol{y}_\mathrm{f})$ and store them in a look-up table.

D. Corrupted Measurements

So far we have assumed that the measurements available to the controller are exact. They may, however, be subject to (typically small) measurement errors. More challenging, they may also be completely off either due to technical errors during transmission or due to malicious attacks on parts of the system. In the following, we extend our approach so that it can tolerate the manipulation of a small number of the available measurements – without the need to know or identify the exact subset of disturbed sensors. Smaller measurement errors can be solved in a similar fashion but are not the focus here.

Now, we first introduce the *true* measurement $\boldsymbol{y}_\mathrm{f}^\mathrm{true}$, which is corrupted by an uncertain additive component $\Delta\boldsymbol{y}_\mathrm{f}$ affecting only k unknown elements of $\boldsymbol{y}_\mathrm{f}^\mathrm{true}$. The measurement available to the controller is then given by

$$\boldsymbol{y}_\mathrm{f} = \boldsymbol{y}_\mathrm{f}^\mathrm{true} + \Delta\boldsymbol{y}_\mathrm{f}, \quad \Delta\boldsymbol{y}_\mathrm{f} \in [\underline{\Delta\boldsymbol{y}}_\mathrm{f}, \overline{\Delta\boldsymbol{y}}_\mathrm{f}]. \tag{7}$$

The j-th entry of $\Delta\boldsymbol{y}_\mathrm{f}$ is zero if the j-th measurement is not manipulated. In addition, the boundaries $\underline{\Delta\boldsymbol{y}}_\mathrm{f}$ and $\overline{\Delta\boldsymbol{y}}_\mathrm{f}$ specify the minimum and maximum plausible measurement deviation. They can, e.g., be computed using the constraints on the state variables and $\boldsymbol{y}_\mathrm{f} = \mathbf{M}_\mathrm{f}\boldsymbol{x}_\mathrm{f}$.

1) Exact formulation: Let $\boldsymbol{u}_\mathrm{f} \in \{0,1\}^L$ be the binary decision variable whose jth-entry is one if the jth-entry of $\boldsymbol{y}_\mathrm{f}$ is corrupted, and zero otherwise. Since only k measurements are affected by $\Delta\boldsymbol{y}_\mathrm{f}$,

$$\mathbf{1}^\mathrm{T}\boldsymbol{u}_\mathrm{f} \leq k \tag{8}$$

has to be fulfilled. Then, the uncertainty set for $\Delta\boldsymbol{y}_\mathrm{f}$ can be expressed as

$$\Delta\boldsymbol{\mathcal{Y}}_\mathrm{f} = \{\Delta\boldsymbol{y}_\mathrm{f} \subset \mathbb{R}^L : \underline{\Delta\boldsymbol{y}}_\mathrm{f} \circ \boldsymbol{u}_\mathrm{f} \leq \Delta\boldsymbol{y}_\mathrm{f} \leq \overline{\Delta\boldsymbol{y}}_\mathrm{f} \circ \boldsymbol{u}_\mathrm{f}\}. \tag{9}$$

Here, $\circ$ denotes the Hadamard product. Using (8), (9), and the given measurement $\boldsymbol{y}_\mathrm{f}$, the maximum impact of $\boldsymbol{x}_\mathrm{f}$ on the i-th constraint of the system, provided that the measurement $\boldsymbol{y}_\mathrm{f}$ has k corrupted elements, can be found for $i \in \{1,...,K\}$ by solving the following mixed-integer linear program (MILP)

$$\begin{aligned} \overline{z}_{\mathrm{f},i} = &\max_{\boldsymbol{x}_\mathrm{f}\in\boldsymbol{\mathcal{X}}_\mathrm{f},\Delta\boldsymbol{y}_\mathrm{f},\boldsymbol{u}_\mathrm{f}} \mathbf{A}_\mathrm{f}^i\boldsymbol{x}_\mathrm{f} \\ &\text{s.t. } \boldsymbol{y}_\mathrm{f} = \mathbf{M}_\mathrm{f}\boldsymbol{x}_\mathrm{f} + \Delta\boldsymbol{y}_\mathrm{f}, \\ &\quad \mathbf{1}^\mathrm{T}\boldsymbol{u}_\mathrm{f} \leq k, \\ &\quad \underline{\Delta\boldsymbol{y}}_\mathrm{f} \circ \boldsymbol{u}_\mathrm{f} \leq \Delta\boldsymbol{y}_\mathrm{f} \leq \overline{\Delta\boldsymbol{y}}_\mathrm{f} \circ \boldsymbol{u}_\mathrm{f}, \\ &\quad \boldsymbol{u}_\mathrm{f} \in \{0,1\}^L. \end{aligned} \tag{10}$$

Once the vector $\overline{\boldsymbol{z}}_\mathrm{f}$ is determined, the value $\boldsymbol{x}_\mathrm{c}$ can be computed as before by solving LP (5).

2) Linear Approximation: Although MILP (10) already provides an efficient procedure to tackle k corrupted measurements, it can be computationally demanding for large K and large dimensions of $\boldsymbol{x}_\mathrm{f}$. To improve the efficiency of the algorithm, we approximate the uncertainty set of $\Delta\boldsymbol{y}_\mathrm{f}$ by relaxing the integer constraint $\boldsymbol{u}_\mathrm{f} \in \{0,1\}^L$ to the box constraints $\mathbf{0} \leq \boldsymbol{u}_\mathrm{f} \leq \mathbf{1}$. In this manner, we can determine the maximum impact of $\boldsymbol{x}_\mathrm{f}$ on the i-th system constraint, $i \in \{1,...,K\}$, for a given measurement $\boldsymbol{y}_\mathrm{f}$ having k corrupted elements via the LP

$$\begin{aligned} \overline{z}_{\mathrm{f},i} = &\max_{\boldsymbol{x}_\mathrm{f}\in\boldsymbol{\mathcal{X}}_\mathrm{f},\Delta\boldsymbol{y}_\mathrm{f},\boldsymbol{u}_\mathrm{f}} \mathbf{A}_\mathrm{f}^i\boldsymbol{x}_\mathrm{f} \\ &\text{s.t. } \boldsymbol{y}_\mathrm{f} = \mathbf{M}_\mathrm{f}\boldsymbol{x}_\mathrm{f} + \Delta\boldsymbol{y}_\mathrm{f}, \\ &\quad \mathbf{1}^\mathrm{T}\boldsymbol{u}_\mathrm{f} \leq k, \\ &\quad \underline{\Delta\boldsymbol{y}}_\mathrm{f} \circ \boldsymbol{u}_\mathrm{f} \leq \Delta\boldsymbol{y}_\mathrm{f} \leq \overline{\Delta\boldsymbol{y}}_\mathrm{f} \circ \boldsymbol{u}_\mathrm{f}, \\ &\quad \mathbf{0} \leq \boldsymbol{u}_\mathrm{f} \leq \mathbf{1}. \end{aligned} \tag{11}$$

V. Application Examples

The proposed algorithm is now demonstrated with simulations of active distribution networks. First, two explanatory distribution feeders of small size are studied. Thereafter, the scalability of our algorithm is verified using a modified version of the IEEE 123 bus test case. The algorithms were implemented in Matlab, using CPLEX as LP/MILP solver, and YALMIP [9] as modeling language.

A. 3 Node Distribution Feeder

Fig. 1 (a) shows a simple distribution feeder with two loads and two photovoltaic (PV) units. The setup – although strongly simplified – resembles a typical situation in today distributions with high PV penetration. The impedance of each line segment is assumed to be $0.03 + \mathrm{j}0.06$ p.u. High PV-infeeds at low loads lead to voltage rises towards the end of the feeder, high loads without PV production to voltage drops. Keeping the nodal voltage levels within $[0.9,\ 1.1]$ p.u. thus represents the relevant operational constraint, while transmission limits are not relevant here.

The PV units generate active power depending on the weather conditions, with maximum capacity of 1 p.u. We assume that the geographically closeness of the PV units leads to strong coupling of their production, i.e., both PV units produce the same power in each time step. This behavior is modeled by the interval uncertainty set shown in Fig. 1 (b). The maximum load at each node is assumed to be 1 p.u., but we limit the joint demand to 50% of the sum of the individual peak demands, resulting in the uncertainty set shown in Fig. 1 (c). The uncertainty set for the combined active power injections is illustrated in Fig. 1 (d).

We assume in this example that the PV units do not inject reactive power to the network, leaving the OLTC of the distribution transformer as the unique controllable actuator to regulate the voltage.

We first study the case in which there is no information available online to set the voltage v_0 via the OLTC, meaning that a constant voltage v_0 should be valid for all active power injections in the uncertainty set. For this setup, the maximum impact of the uncertain active power injections on the system constraints is computed via LP (4). Subsequently, we solve LP (5) and obtain $\beta > 0$. This means that the current actuator/sensor equipment does not allow for the design of an admissible control law, i.e., there is no constant v_0 guaranteeing feasible system operation in all cases.

Now we integrate the measurement of the nodal active power at the root bus into the control system, which is a common local measurement available to OLTC controllers. The new controller setup admits an admissible control law since by applying the proposed two-stage algorithm we can determine a feasible value v_0 for each possible power measurement p_0 in the range $[-1,\ 2]$ p.u., see Fig. 1 (e). In case of high PV generation, voltage v_0 is set to its lower bound, independently of the load values. In contrast, when there is no PV generation and one of the loads reaches its peak value, voltage v_0 is set to 1.09 p.u., close to its maximum allowed value. As expected, the voltage v_0 increases gradually with the power p_0 provided by the transformer.

Unlike the following examples, this small test case could be solved intuitively, but serves to validate the proposed approach.

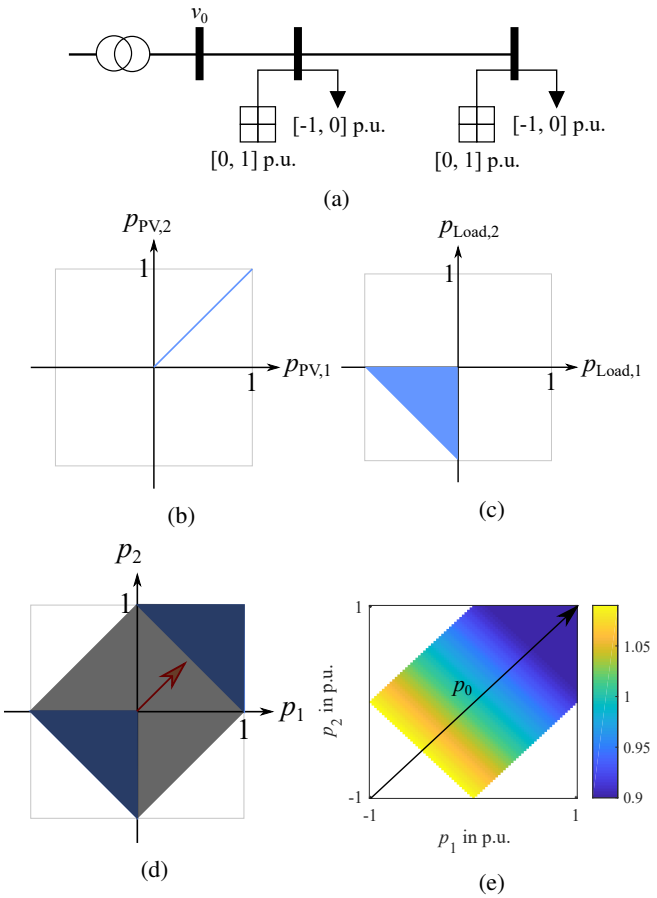

Fig. 1: Exemplary active distribution feeder subject to uncertain active power loads and coupled PV production. (a) Topology of the network with specified operation limits for loads and PV units. (b) The blue line corresponds to the uncertainty set for the active power generated by the PV units. (c) The blue region models the uncertainty for the loads. (d) The uncertainty set for the active power injections (shaded) is obtained by combining the sets (a) and (b). (e) Optimal voltage set point v_0 as a function of the active power p_0 provided by the distribution transformer.

B. 11 Node Distribution Feeder

Now we apply the control algorithm proposed in IV to simulate the operation of the 11 node feeder shown in Fig. 2 for one day. The system has active power loads of up to 1 p.u. connected to nodes $\{1, 2, 4, 8, 9\}$, PV units with capacity of 1 p.u. are connected to nodes $\{3, 5, 6, 7, 10\}$. With exception to the PV unit at node 7, which has a reactive power capacity of ± 0.2 p.u., all remaining PV units operate with a power factor of 1. The impedance of each line segment is assumed as $0.002 + \mathrm{j}0.006$ p.u.

The voltage at node 0 is controlled via the OLTC within the operation interval of $[0.9, 1.1]$ p.u. In addition, the reactive power injection of the PV unit at node 7 can also be controlled. The control system has access to the measurement of the nodal voltages at nodes $\{3, 7, 10\}$ as well as the active power provided by the transformer.

As above, the production of the PV units is assumed to be coupled. The PV generation follows the profile of a sunny day as shown in Fig. 3 (a). Power consumptions are modeled

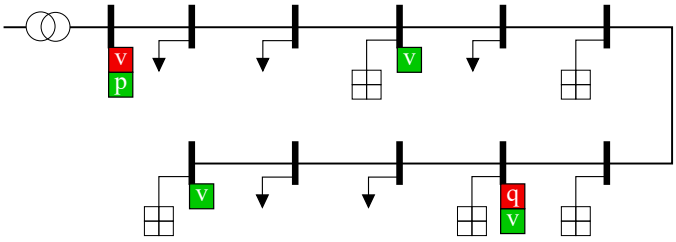

Fig. 2: 11 node distribution feeder with 5 loads and 5 coupled PV units. The controller sets the OLTC voltage v_0 and the reactive power injection of the PV unit at node 7 (red boxes) based on the available measurements (green boxes).

as individual random processes with uniform distribution. Fig. 3 (b) shows the resulting load profiles together with the total load over time. The controller determines new control set points every 5 minutes.

Initially, the controller is designed for the case of having non-corrupted measurements. Using the proposed minimal action control algorithm based on LP (4), we obtain the optimal trajectory for v_0 depicted in Fig. 3 (c). In this scenario, the voltage at the distribution transformer has to be adjusted only two times. As expected, the maximum nodal voltage in the network coincides with v_0 during the hours of low PV generation. In contrast, the value of v_0 corresponds to the minimum nodal voltage in the network during the peak PV generation hours. During the day, the lowest nodal voltage levels were reported at nodes $\{0, 1, 2, 4, 8, 9, 10\}$, and the highest at nodes $\{0, 5, 6, 7, 10\}$. This indicates that the identification of critical nodes in the feeder is not trivial when having a high, non-uniformly spread penetration of decentralized generation in the network.

Subsequently, we design the controller to support the manipulation of up to $k = 1$ measurement, which is unknown to the controller. We define the interval boundaries of $\Delta\mathcal{Y}_{\mathrm{f}}$ for the voltage measurements as 0.5 p.u. in both directions. To check the validity of the approach, we artificially alter the voltage sensor at bus 10 with a constant offset of 0.3 p.u. in our simulation. This voltage manipulation is unknown to the controller.

Interestingly, the obtained control solution for v_0 using the MILP formulation (10) for dealing with corrupted measurements is almost identical as the solution for the undisturbed case. This demonstrates well that our proposed approach is robust to this large distortion.

When computing controller values based on the relaxed LP formulation (11) for dealing with corrupted measurements we obtain a slightly different solution for the v_0 values, see Fig. 3 (d). Due to the relaxation, the size of the uncertainty set increases and the computed the worst-case upper and lower voltages show a wider corridor than before. This forces the algorithm to adapt the control values more often. Nevertheless, the voltage is adapted only 4 times during the day.

Fig. 3 (e) shows the resulting trajectories for the reactive power to be injected by the PV unit connected at node 7. By choosing one of the approaches, users can make their preferred choice in the trade-off between the slightly higher computational requirements for the MILP approach and its superior solution quality.

C. Modified IEEE 123 Bus Test Feeder

To validate the scalability of the proposed control algorithms, we briefly present its application to a modified version of the IEEE 123 bus test case [10], see Fig. 4 (a). We install a total of 36 PV units with a capacity of 50 p.u. in the grid, assuming power factor 1 for all of them. The control center is able to control the voltage v_0 at the main tranformer as well as the voltage regulators at nodes 9, 25, and 118. The measurement set consists of the active power injection at node 0 and the nodal voltages at a few of the PV units that are assumed to be connected to the control center. A maximum of $k = 2$ sensors are assumed to be subject to exogenous manipulation with an uncertainty set $\Delta\mathcal{Y}_{\mathrm{f}}$ defined identically as in the previous section. As before, the PV production is taken as coupled, each of them following the generation profile shown in Fig. 3 (a). The active and reactive power loads are modeled uniformly random, with peak values as specified in [10]. The average total active and reactive loads for the simulated time window are 1500 p.u. and 500 p.u., respectively. The simulated voltage measurements available to the controller are manipulated for two sensors, via an offset of 0.4 p.u. The disturbed subset is unknown to the controller.

Every 5 min, the controller determines the value of the controlled variables for the given measurements to guarantee nodal voltage levels within the interval $[0.9,\ 1.1]$ p.u.. By applying the proposed minimal action control concept based on MILP (10), we obtain the trajectories for the controlled variables depicted in Figs. 4 (b) and (c). Observe how the minimum and maximum voltages, that the controller must assume possible in the grid due to its uncertainty assumptions, are closed to the operational limits during almost the whole simulation day. This results in 5 switching operations during the day. The voltage regulators change their value synchronously with v_0. The solver time for each iteration of the control algorithm is about 9 secs on an i5 notebook with 8GB of RAM.

VI. Concluding Remarks & Outlook

This paper presents a novel robust control technique for constrained static linear systems based on two-stage optimization. The potential of the proposed ideas is demonstrated in its application to voltage regulation in active distribution networks subject to corrupted measurements. Future work will focus on the design of control laws tolerating also the targeted manipulation of a small subset of the actuators.

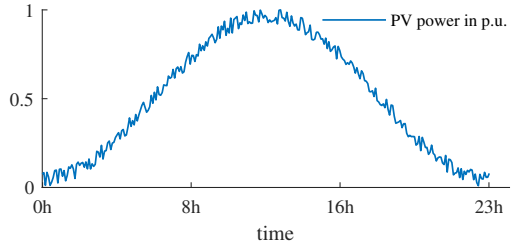

(a) Generation profile for each PV unit during a sunny day.

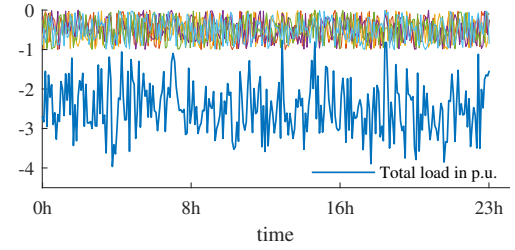

(b) Load profiles taken from a uniform random process.

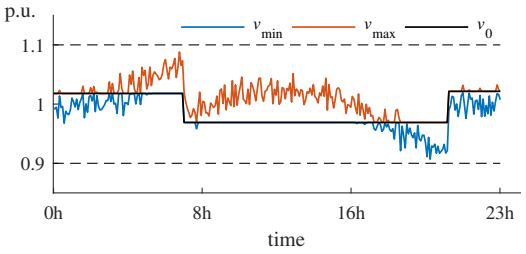

(c) OLTC voltage v_0 and maximal/minimal possible voltages throughout the grid assuming correct, see LP (4), or corrupted, see MILP (10) with $k = 1$, measurements.

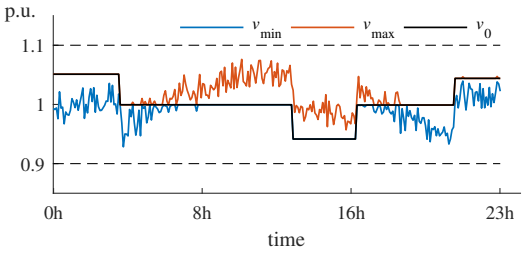

(d) OLTC voltage v_0 and maximal/minimal possible voltages throughout the grid assuming corrupted measurements, see LP (11) with $k = 1$.

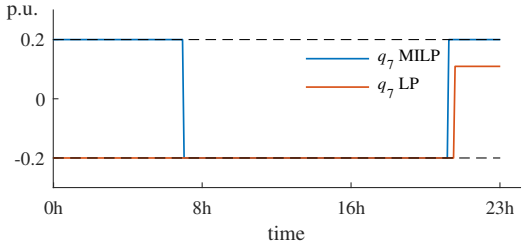

(e) Reactive power set points q_7 corresponding to the plots (c) and (d).

Fig. 3: Simulation of the robust minimal action control for the 11 node distribution feeder of Fig. 2 during a sunny day.

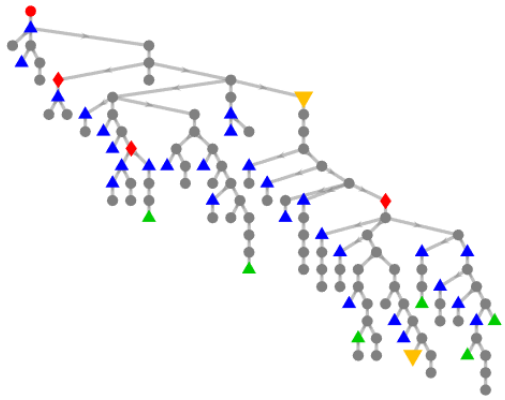

(a) Topology of the modified IEEE 123 bus test case.

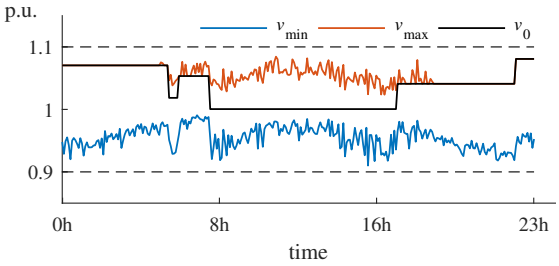

(b) OLTC voltage v_0 and maximal/minimal possible voltages throughout the grid assuming up to two corrupted measurements, see MILP (10) with $k = 2$.

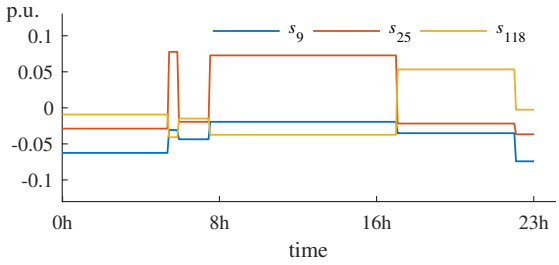

(c) Corresponding control values for (s_9, s_{25}, s_{118}).

Fig. 4: Simulation of the VVC control for the modified version of the IEEE 123 bus test case during a sunny day. In (a) the red circle represents the root node, whose nodal voltage is controlled and active power measured. Red diamonds symbolize locations of controllable voltage regulators. Nodes with PV units are marked with the blue, green, or orange triangles. Green and orange marks indicate that the local voltage is available to the control center. Orange implies that the measurement is distorted.

References

[1] N. Mahmud and A. Zahedi, "Review of control strategies for voltage regulation of the smart distribution network with high penetration of renewable distributed generation," *Renewable and Sustainable Energy Reviews*, vol. 64, pp. 582 – 595, 2016.

[2] N. Daratha, B. Das, and J. Sharma, "Coordination between oltc and svc for voltage regulation in unbalanced distribution system distributed generation," *IEEE Transactions on Power Systems*, vol. 29, no. 1, pp. 289–299, 2014.

[3] P. Li, H. Ji, C. Wang, J. Zhao, G. Song, F. Ding, and J. Wu, "Coordinated control method of voltage and reactive power for active distribution networks based on soft open point," *IEEE Transactions on Sustainable Energy*, vol. 8, no. 4, pp. 1430–1442, 2017.

[4] F. Bignucolo, R. Caldon, and V. Prandoni, "Radial MV networks voltage regulation with distribution management system coordinated controller," *Electric Power Systems Research*, vol. 78, no. 4, pp. 634 – 645, 2008.
[5] T. Niknam, M. Zare, and J. Aghaei, "Scenario-based multiobjective volt/var control in distribution networks including renewable energy sources," *IEEE Transactions on Power Delivery*, vol. 27, no. 4, pp. 2004–2019, 2012.
[6] P. Li, C. Zhang, Z. Wu, Y. Xu, M. Hu, and Z. Dong, "Distributed adaptive robust voltage/var control with network partition in active distribution networks," *IEEE Transactions on Smart Grid*, vol. 11, no. 3, pp. 2245–2256, 2019.
[7] E. Mora and F. Steinke, "On the minimal set of controllers and sensors for linear power flow," *Electric Power Systems Research*, vol. 190, p. 106647, jan 2021.
[8] M. E. Baran and F. F. Wu, "Optimal capacitor placement on radial distribution systems," *IEEE Transactions on Power Delivery*, vol. 4, no. 1, pp. 725–734, 1989.
[9] J. Löfberg, "YALMIP: A toolbox for modeling and optimization in matlab," in *In Proceedings of the CACSD Conference*, Taipei, Taiwan, 2004.
[10] "IEEE 123 bus test case." [Online]. Available: https://site.ieee.org/pes-testfeeders/resources/